Energy & Environmental Science

www.rsc.org/ees

Volume 5 | Number 9 | September 2012 | Pages 8401–8764

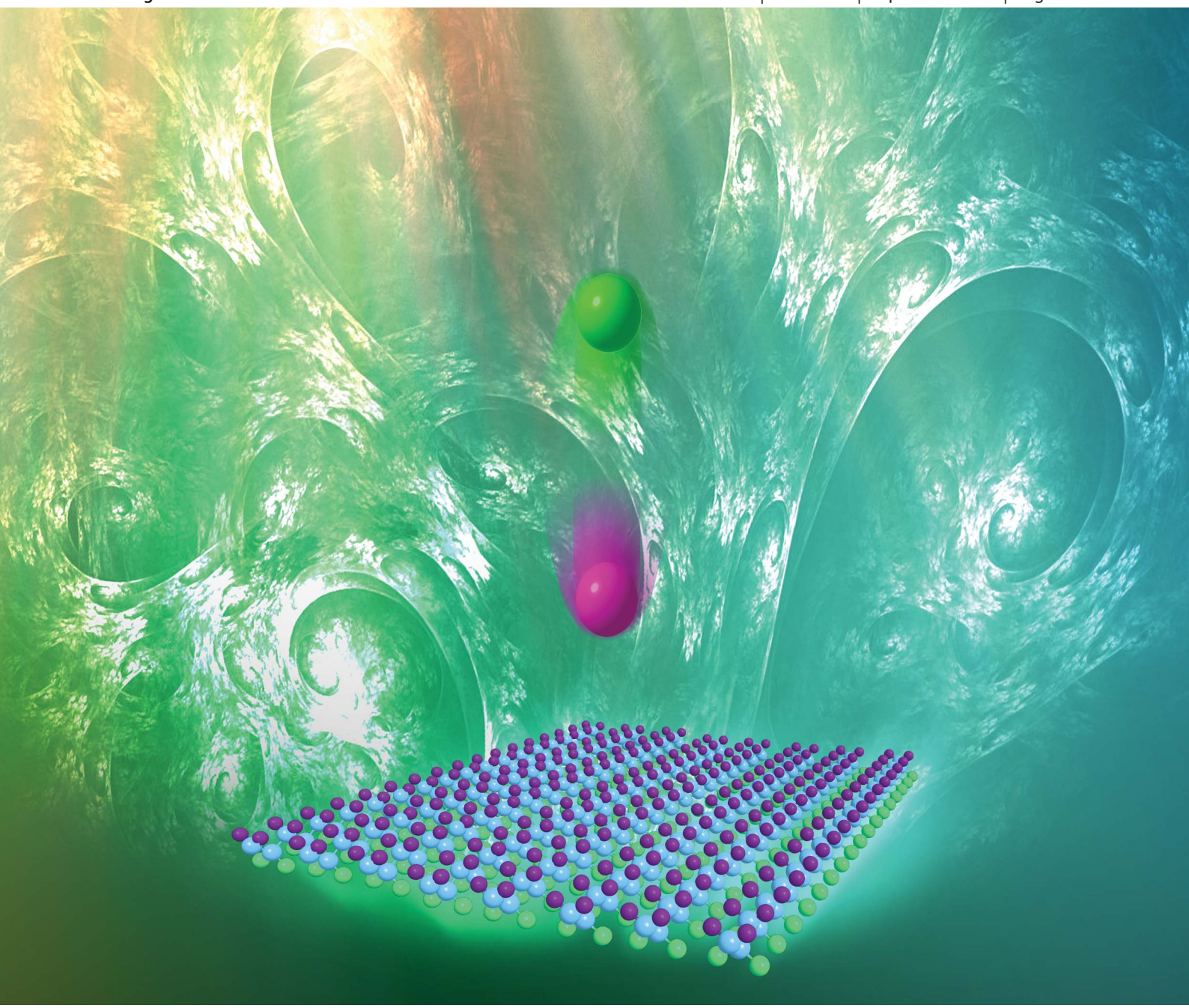

ISSN 1754-5692

RSC Publishing

HOT ARTICLE

Jinsong Huang *et al.*

Understanding the effect of ferroelectric polarization on power conversion efficiency of organic photovoltaic devices

Energy & Environmental Science

Dynamic Article Links

Cite this: *Energy Environ. Sci.*, 2012, **5**, 8558

www.rsc.org/ees

PAPER

Understanding the effect of ferroelectric polarization on power conversion efficiency of organic photovoltaic devices

Yongbo Yuan,†[ab] Pankaj Sharma,†[bc] Zhengguo Xiao,†[ab] Shashi Poddar,[bc] Alexei Gruverman,[bc] Stephen Ducharme[bc] and Jinsong Huang*[ab]

Received 30th April 2012, Accepted 29th May 2012
DOI: 10.1039/c2ee22098a

It is demonstrated that the power conversion efficiency (PCE) of organic photovoltaic devices can be increased by inserting an ultrathin film of a ferroelectric co-polymer, poly(vinylidenefluoride-trifluoroethylene) (P(VDF-TrFE)), at the metal–organic interface, due to an enhancement of the charge extraction efficiency. Specifically, the effect of P(VDF-TrFE) crystallinity on its function in ferroelectric organic photovoltaic (FE-OPV) devices has been studied by several methods. Highly crystalline and amorphous P(VDF-TrFE) films have been prepared by the Langmuir–Blodgett method and spin-coating from acetone solution, respectively. The polymer solar cell devices with a crystalline P(VDF-TrFE) interfacial layer at the cathode have larger PCE than the structures with amorphous P(VDF-TrFE) and have the unique feature of switchable diode polarity and photovoltaic performance controlled by external applied voltage pulses. The obtained results confirm that the spontaneous polarization of the ferroelectric P(VDF-TrFE) layer is responsible for the enhancement of PCE in FE-OPV devices and that a highly crystalline ferroelectric polymer film is required to observe the enhancement of PCE. Amorphous P(VDF-TrFE) films act as regular dielectric layers with a little poling effect on device PCE. The polarization of P(VDF-TrFE) is shown to be stable, and the photogenerated charges could be collected efficiently by the cathode rather than being compensated.

1. Introduction

Organic photovoltaic (OPV) research has developed rapidly during the last few years. The highest reported power conversion efficiency (PCE) has been increasing steadily, exceeding 10%.[1] Several innovative approaches have been used to increase the OPV efficiency, including optimization of morphology by thermal and/or solvent annealing, optimization of electrode work function, reduction of the band-gap of the light absorbing polymers, development of stacking/tandem structures to

[a]*Department of Mechanical and Materials Engineering, University of Nebraska-Lincoln, Lincoln, Nebraska 68588-0656, USA. E-mail: jhuang2@unl.edu*
[b]*Nebraska Center for Materials and Nanoscience, University of Nebraska-Lincoln, Lincoln, Nebraska 68583-0298, USA*
[c]*Department of Physics and Astronomy, University of Nebraska-Lincoln, Lincoln, Nebraska 68588-0299, USA*
† These authors contributed to this work equally.

Broader context

Organic photovoltaic (OPV) cells with polymer-fullerene bulk heterojunction are promising candidates for future low-cost, high-performance energy sources. The highest reported power conversion efficiency (PCE) has exceeded 10%. Although the highest internal quantum efficiency of one or two materials can approach 100%, the inefficient charge extraction from the light absorbing layer is still a major challenge for many semiconductor polymers, including low bandgap polymers recently developed. Recently, we reported a method to increase the charge pair separation and charge extraction efficiency using a permanent electric field of an ultrathin layer of ferroelectric co-polymer poly[(vinylidenefluoride-trifluoroethylene] (P(VDF-TrFE)) introduced at the interface between the electrode and a semiconductor layer, which enhances the power conversion efficiency (PCE) of several types of OPV by up to 200% (*Nat. Mater.*, **10**, 296, 2011). In this paper, we studied the effect of P(VDF-TrFE) crystallinity on the performance of a ferroelectric OPV (FE-OPV). It was shown the enhanced PCE and the switchable FE-OPVs are well connected to the ferroelectric nature of the P(VDF-TrFE) crystallinity. The results highlight the P(VDF-TrFE) crystallinity as a critical issue for FE-OPVs and provide guidance for the fabrication of high performance FE-OPV devices.

combine the high bandgap and low bandgap materials, *etc.*[2–5] Despite the fact that the highest internal quantum efficiency of one or two materials can approach 100% for some devices with special structure,[6] a major challenge for many semiconductor polymers, including low bandgap polymers recently developed, is the inefficient charge extraction from the light absorbing layer. A significant portion of energy is lost to heat due to the non-radiative recombination of charges or charge transfer excitons (CTEs).[7–11]

Recently, we reported a method to increase the CTE separation and charge extraction efficiency using a permanent electric field of an ultrathin layer of a ferroelectric co-polymer, poly(vinylidenefluoride-trifluoroethylene) P(VDF-TrFE), introduced at the interface between the electrode and a semiconductor layer. After poling in the proper direction, polarization charges on P(VDF-TrFE) induce a strong internal electric field in the semiconducting active layer. The induced electric field significantly enhances the CTE dissociation and increases the charge collection efficiency. The PCEs of several types of OPV were increased by up to 200% – the highest reported value for the devices using the same type of active materials.[12] In subsequent work, the ferroelectric polarization of P(VDF-TrFE) has been used to shift the relative donor and acceptor energy levels to increase the open circuit voltage (V_{oc}) of OPV without interrupting the charge transfer and collection.[13] On the other hand, it was argued[14] that the observed PCE enhancement was caused by an electrochemical reaction between Al and P(VDF-TrFE) under an applied electric field rather than by the polarization of the P(VDF-TrFE) layer. This argument was put forward based on apparently the same behavior shown by the OPV devices with the P(VDF-TrFE) layer and non-ferroelectric polymer. In this paper, we report the effect of P(VDF-TrFE) crystallinity on the performance of a ferroelectric OPV (FE-OPV). The obtained results provide guidance for the fabrication of high performance FE-OPV devices and explain the contradictory results reported in ref. 14. The crystalline P(VDF-TrFE) reported here can be used as a universal interfacial layer for both cathode and anode.

2. Experimental

FE-OPV device fabrication and measurement. Cleaned indium tin oxide (ITO) substrates were firstly treated by UV-ozone for 10 minutes. Poly(3,4-ethylenedioxythiophene)–polystyrenesulfonic acid (PEDOT:PSS, Baytron-P 4083) was then spun onto ITO substrates at a speed of 3000 rpm. Regioregular poly(3-hexylthiophene) (P3HT) and phenyl-C61-butyric acid methyl ester ($PC_{60}BM$) were purchased from Rieke Metals Inc. and Nano Carbon Inc. respectively, they were used as received. The films have been deposited on the P3HT:$PC_{60}BM$ layer on a glass/ITO substrate. Both materials were dissolved in 1,2-dichlorobenzene (DCB) at 35 mg ml^{-1} and blended in a mass ratio of 1 : 1 and stirred for about 15 hours at 40 °C. Then the solution was spun on PEDOT:PSS at a speed of 800 rmp for 20 s inside the glovebox. Ultrathin P(VDF-TrFE 70:30) dipole layers were deposited on the P3HT:$PC_{60}BM$ layers by spin-coating 0.2% P(VDF-TrFE) (dissolved in acetone) at a speed of 6000 rpm for 60 s or by Langmuir–Blodgett (LB) coating. The details of the LB coating process can be found elsewhere.[12] The LB films were annealed at 135 °C for 30 min, and the spun films were annealed at 90 °C for 10 min as reported in ref. 14. The FE-OPV device fabrication was finished by thermally evaporating 100 nm thick Al for regular solar cell devices, or 30 nm Au for switchable diode devices.

Electrical characterization. The current–voltage (*I–V*) characteristics of the devices were measured in the glove box ($O_2 < 0.1$ ppm) under simulated AM 1.5G irradiation (100 mW cm^{-2}) using a xenon-lamp-based solar simulator (Oriel 96000 150W Solar Simulator) which is calibrated by a KG5 filtered-silicon detector. For the P(VDF-TrFE) dipole relaxation measurement, the devices were fixed on a metallic platform and illuminated by 0.3 sun (30 mW cm^{-2}) irradiation. Then the devices were heated by attaching a 135 °C hot metal block for 25 s without applying a bias to depolarize the dipole and then the metal blocks were removed. The photocurrents were monitored *in situ* during the whole process.

Domain visualization has been performed using piezoresponse force microscopy (PFM) by applying a high-frequency modulating voltage (200–600 kHz, 1.0–1.5 V) to the Pt–Ti-coated silicon (Mikromasch) or Au-coated SiN tips (Olympus). Local piezoelectric hysteresis loops were measured in fixed locations on the film as a function of a dc bias superimposed on ac modulation voltage.

Structural characterization. In the X-ray diffraction (XRD) measurement, both the P(VDF-TrFE) LB film (50 ML) and spun film (150 nm) were deposited on bare Si substrates. The XRD data were taken with a Rigaku D/Max-B X-ray diffractometer with Bragg–Brentano parafocusing geometry, a diffracted beam monochromator, and a conventional copper target X-ray tube set to 40 KV and 30 mA. The wavelength of the X-rays is 1.544 Å (Cu Kα).

3. Results and discussion

3.1 Crystallinity of the P(VDF-TrFE) films fabricated by LB and spin coating methods

To determine the effect of the ferroelectric polymer layer on the performance of the OPV device, it is essential to fabricate P(VDF-TrFE) of high crystallinity,[15] and then perform thorough electrical characterization to verify its ferroelectric nature. For this reason, we fabricated two types of OPV devices, differing only in the method of deposition of the P(VDF-TrFE) copolymer film. The P(VDF-TrFE) films were fabricated by two different methods, LB deposition from a water subphase and spin-coating from acetone solution, as described in ref. 14. The films were deposited on an OPV nanocomposite layer composed of P3HT and $PC_{60}BM$ which was deposited by spin coating on an ITO/glass substrate. The LB-deposited 2 monolayer (ML) P(VDF-TrFE) films with an average thickness of 3.4 nm were annealed for 30 minutes at 135 °C to optimize their crystallinity.[16–18] The P(VDF-TrFE) films formed by spin coating with an average thickness of 3.2 nm were annealed at a lower temperature of 90 °C for 10 min as described in ref. 14. Typical morphology of the P(VDF-TrFE) films fabricated by these two deposition methods is illustrated in Fig. 1a. The samples fabricated by these two deposition methods with a thickness around 150 nm were firstly characterized by XRD study. LB deposition results in fabrication of highly crystalline P(VDF-TrFE) films as thin as

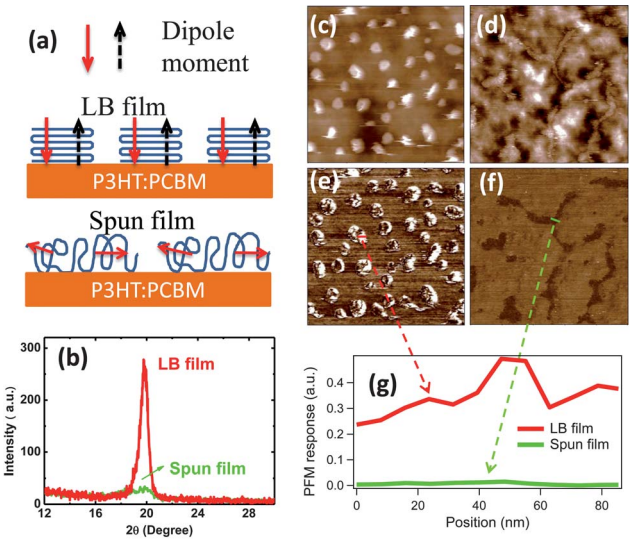

Fig. 1 (a) An illustration of the morphology of the LB and spun P(VDF-TrFE) films. (b) XRD spectra of a 50 ML P(VDF-TrFE) LB film and a spun P(VDF-TrFE) film (~150 nm) on Si substrate; (c) topography of a P(VDF-TrFE) LB film (2 μm × 2 μm); (d) topography of a P(VDF-TrFE) spun film (5 μm × 5 μm); (e) PFM amplitude images of a P(VDF-TrFE) LB film; and (f) PFM response mapping images of the P(VDF-TrFE) spun film on P3HT:$PC_{60}BM$ surface. (g) Comparison of the PFM amplitude of the P(VDF-TrFE) LB film and spun film on the marked positions in (e–f).

1 nm,[19] evident by the strong and sharp combined (110)–(020) peak shown in Fig. 1b.[20] The spun P(VDF-TrFE) films show a very weak (110)–(020) diffraction peak, which indicates that these films have much poorer crystallinity. This difference is not surprising, because the boiling point of acetone (56 °C) is too low to form a crystalline copolymer due to the quick solvent evaporation in the spin coating process. In addition, the spun P(VDF-TrFE) films must be annealed above the ferroelectric–paraelectric transition temperature, which is over 100 °C for the 70% VDF copolymer, to achieve high crystallinity.[21]

3.2 Ferroelectric properties of the LB and spun P(VDF-TrFE) films

To further investigate the role of the film fabrication procedure on the ferroelectric properties, the P(VDF-TrFE) films have been tested by PFM.[22,23] The results of these studies are shown in Fig. 1c–f. The LB P(VDF-TrFE) film (2 ML) shows strong PFM contrast while the spun P(VDF-TrFE) film shows barely any PFM response, which is consistent with its low crystallinity. XRD and PFM imaging data clearly show that the spun P(VDF-TrFE) films have very weak ferroelectricity, and therefore can function only as a regular dielectric layer.

The ferroelectric nature of the LB P(VDF-TrFE) films has been further confirmed by inducing polarization reversal using the electrically biased PFM tip (Fig. 2). A ±10 V, 1 s voltage pulse supplied by the PFM tip can switch the polarization of the P(VDF-TrFE) crystallites up and down, as is clearly observed in the PFM images. Saturated hysteresis loops measured by PFM in LB P(VDF-TrFE) on P3HT:$PC_{60}BM$ are shown in Fig. 2g–h.

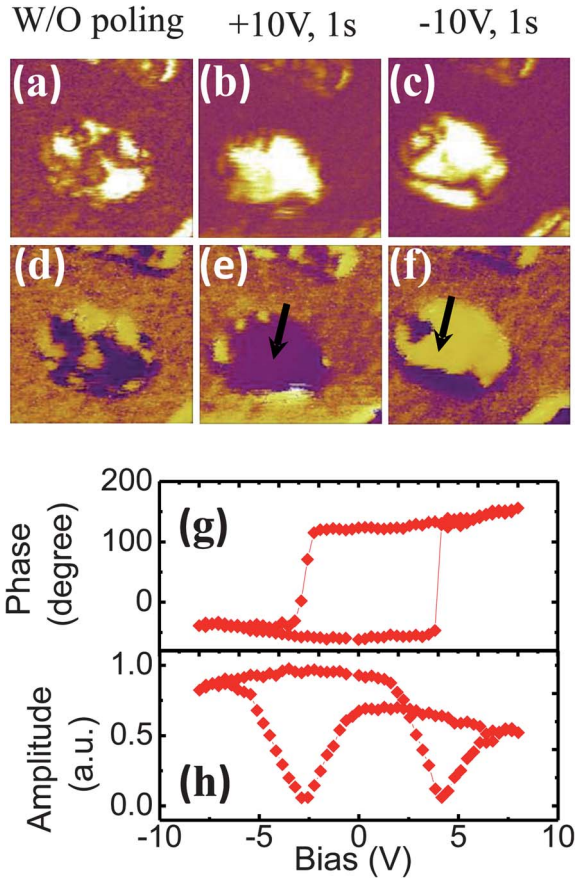

Fig. 2 PFM amplitude (a–c) and phase images (d–f) of the domain structure in the P(VDF-TrFE) nanomesa on P3HT:$PC_{60}BM$ before and after application of positive or negative voltage pulses. (g–h) PFM hysteresis loops (phase and amplitude) of an unscreened P(VDF-TrFE) domain on a P3HT:$PC_{60}BM$ layer.

3.3 Switch capability of the devices with LB and spun P(VDF-TrFE) interlayers

The switchable polarization of ferroelectric material results in a switchable photovoltaic and diode effect, which is a unique characteristic of a ferroelectric photovoltaic device.[24,25] We first compared the performance of the devices with crystalline and amorphous P(VDF-TrFE), *i.e.*, prepared by LB deposition and spin coating, respectively, on the three states: as-grown, positively poled (the device is reverse biased) and negative poled (the device is forward biased). The device structure of ITO/PEDOT:PSS (25 nm)/P3HT:$PC_{60}BM$ (150 nm)/P(VDF-TrFE) (2 ML)/Al (100 nm) is the same as previously reported.[12] As shown in Fig. 3a and b, the performance of the device with crystalline P(VDF-TrFE) changes dramatically with different poling states (as previously demonstrated in ref. 12 and 13) while the device with amorphous P(VDF-TrFE) shows little variation of photocurrent in these three states. The device with crystalline P(VDF-TrFE) LB film has an enhanced PCE of 3.4% after positive poling and suppressed PCE of 1.4% after negative poling the P(VDF-TrFE) layer. In contrast, the PCE of the device with amorphous P(VDF-TrFE) spun film has much smaller difference between 2.5% (enhanced) and 2.0% (suppressed) after positive

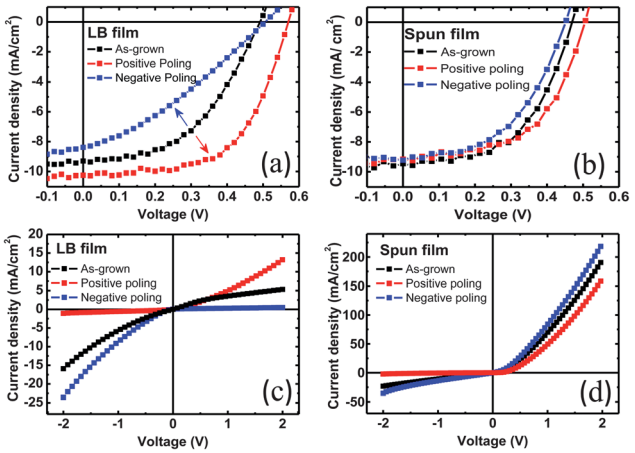

Fig. 3 Comparison of device performance with P(VDF-TrFE) as interfacial layers by LB (a) and spin coating (b) with a device structure of ITO/PEDOT/P3HT:$PC_{60}BM$/P(VDF-TrFE)/Al. Comparison of switching capability of the devices with crystalline (c) and amorphous P(VDF-TrFE) (d) at both cathode and anode with a device structure of ITO/P(VDF-TrFE)/P3HT:$PC_{60}BM$/P(VDF-TrFE)/Au.

and negative poling, respectively. It is thus concluded that the amorphous P(VDF-TrFE) dielectric film acts primarily as a charge blocking layer, although the relatively small ferroelectric fraction may also contribute to the change. Actually, the observed small tunability of photocurrent in amorphous P(VDF-TrFE) device can be explained by the partial crystallization of P(VDF-TrFE) upon thermal annealing.

To observe more distinct current switching capability of FE-OPV devices, we inserted P(VDF-TrFE) films, prepared by both LB and spin coating methods, on *both* the cathode and anode sides with a device structure of ITO/P(VDF-TrFE) (3.4 nm by LB coating, or 3.2 nm by spin coating)/P3HT:$PC_{60}BM$ (150 nm)/P(VDF-TrFE)/Au (30 nm). Since Au and ITO have very similar work functions, the dipole direction of P(VDF-TrFE) determines the diode direction of the device. Fig. 3c and d show the dark current of the two devices under the three states. The diode conductance direction of the device with crystalline P(VDF-TrFE) was reversed by the switching pulses, while the conductance direction of the device with amorphous P(VDF-TrFE) remained unchanged. This result further confirms that crystalline P(VDF-TrFE) with robust switchable polarization is required to enhance the efficiency of the FE-OPV devices.

3.4 Stability of the polarization in P(VDF-TrFE)

To be of practical use in a FE-OPV device, polarization of the ferroelectric layer needs to be stable for long periods, both in the dark and under illumination. It has been shown in our earlier work that the nanometer-thick nanocrystallites of P(VDF-TrFE) on the doped silicon substrate exhibit stable polarization over a very long period of time (>1 month) even without any top electrode.[26] Strong polarization retention (up to several days at least) was also reported for P(VDF-TrFE) nanoislands covered with a nanometer-thick insulating film.[17,20] The photocurrent output stability of FE-OPV devices with positively poled crystalline P(VDF-TrFE) in a device structure of ITO/PEDOT:PSS (25 nm)/P3HT:$PC_{60}BM$ (150 nm)/P(VDF-TrFE) (2 ML)/Al (100 nm) was measured over a period of more than two weeks. The measurements showed only minimal decay (10%) both for the open circuit voltage and short circuit current (Fig. 4). This weak decay in principle may be caused by a slight depolarization of P(VDF-TrFE), but more likely to be induced by other factors such as degradation of the semiconductor polymers and oxidation of the electrodes, since the devices without the ferroelectric layer also show a similar degradation rate in our lab and those reported elsewhere.[27–29] During the stability test, the devices were kept in the dark and the whole poling process was conducted in the dark.

3.5 Can the polarization charge be screened by the photocurrent?

The polarization of the ferroelectric layer affects the distribution of the charges in the semiconductor layer in the FE-OPV. A simple estimation shows that the photogenerated charge density in an OPV is too small to compensate the polarization charge on the P(VDF-TrFE) surface: the photogenerated charge density measured by charge extraction in real P3HT:$PC_{60}BM$ device under 1 sun illumination is about 0.5–2.8 $\times$ 10^{16} cm^{-3} from zero bias to open circuit voltage,[30] which corresponds to a total sheet charge density in the range of 1.2–6.7 $\times$ 10^{-4} C m^{-2} for an active layer thickness of 150 nm, assuming a uniform charge distribution. This charge density is three orders of magnitude smaller than the polarization charge density of 0.1 C m^{-2} at the P(VDF-TrFE) surface.[31] Therefore, unless the photogenerated charges accumulate at the P(VDF-TrFE)/semiconductor interface over

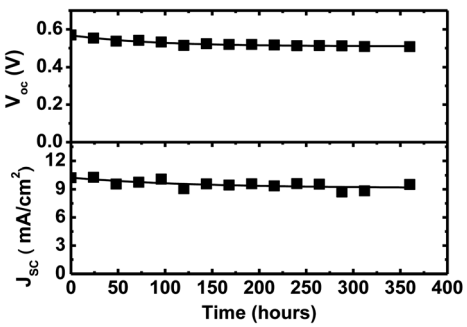

Fig. 4 Variations of the open circuit voltage and short circuit current in the FE-OPV structure over two weeks of observation.

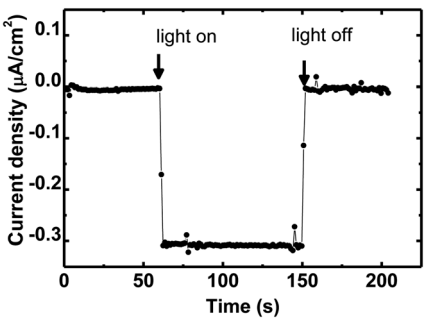

Fig. 5 Short circuit current of LB P(VDF-TrFE) FE-OPV under 3 μW cm^{-2} illumination.

time, in which case the PCE would steadily decrease, the compensation of the polarization charge of P(VDF-TrFE) by the instant photogenerated charges is negligible. In order to find out whether the photogenerated charges accumulate at the P(VDF-TrFE)/semiconductor interface and gradually compensate the polarization charges, we monitored the photocurrent of the FE-OPV under a weak illumination of 3 μW cm^{-2} over a long time scale. If all the photogenerated charges were accumulated at the P(VDF-TrFE)/semiconductor interface, the device needs to be illuminated for 30 s to generate enough charges to completely screen the P(VDF-TrFE) polarization charge. The FE-OPV device was poled right before the testing. Previous results show that the retention time of P(VDF-TrFE) polarization is long enough to guarantee its polarization to be stable during this testing process. If the polarization charges are completely compensated by the photogenerated charges, a decrease in photocurrent is expected after screening. However, as shown in Fig. 5, the device photocurrent is constant during the 90 s of observation. This result thus excludes the accumulation of significant photogenerated charge at the P(VDF-TrFE)/semiconductor interface. This negligible charge accumulation is due to the efficient charge collection at the cathode interface, which is proved by the very high short-circuit current density of the FE-OPV devices.[12]

3.6 Direct correlation of photocurrent with polarization in P(VDF-TrFE)

The next experiment further highlights the essential role of the ferroelectric polarization in enhancing device efficiency. The positively poled ferroelectric layer was partially depolarized by heating it up to 135 °C into the paraelectric phase for 25 seconds and then cooling back to room temperature under zero bias. As shown in Fig. 6a, the photocurrent of the device with crystalline LB P(VDF-TrFE) dropped by 5–10% as a result of dipole misalignment after annealing. In contrast, the photocurrent of the device with amorphous P(VDF-TrFE) is found to be almost the same before and after annealing. The observed bump in the current–time curve during the heating process is probably due to the thermally assisted charge transport.[7] The photocurrent of the device with crystalline P(VDF-TrFE) is still higher than that with amorphous P(VDF-TrFE) after thermal annealing, which might be caused by the incomplete depolarization of P(VDF-TrFE) or partial pinning of the dipoles by P3HT:PC_{60}BM and aluminum oxide.[12] The reduced photocurrent of the device with a crystalline P(VDF-TrFE) interlayer can be explained by the loss of polarization of P(VDF-TrFE) upon thermal annealing without field cooling. The device with an amorphous P(VDF-TrFE) interlayer is not affected by the thermal annealing process because there is no aligned polarization in the amorphous P(VDF-TrFE). These scenarios are illustrated in Fig. 6b. This experiment is additional strong evidence that efficiency improvement in FE-OPV is caused by ferroelectricity of the inserted crystalline P(VDF-TrFE) layer.

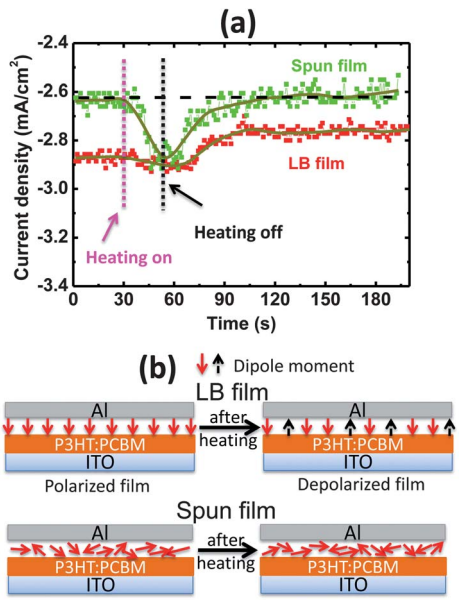

Fig. 6 (a) *In situ* monitoring of the variations in the photocurrent (under 30 mW cm^{-2} illumination) upon annealing to induce depolarization of the ferroelectric layer. (b) Illustration of the dipole rearrangement in P(VDF-TrFE) LB and spun films as a result of annealing.

4. Conclusion

In conclusion, it has been shown that the observed enhancement of PCE of the OPV devices with an inserted thin layer of P(VDF-TrFE) is caused by the ferroelectric polarization of the polymer. It is then critical to fabricate highly crystalline P(VDF-TrFE) films to utilize their ferroelectric properties in FE-OPVs. Amorphous P(VDF-TrFE) films show almost no ferroelectricity and act as regular dielectric layers in the OPV devices, which generally reduces the device efficiency due to the increased contact resistance. Polarization of crystalline P(VDF-TrFE) has been shown to be very stable at the semiconducting polymer/Al interface. The instant photocurrent in FE-OPV devices is too small to screen the polarization charges of P(VDF-TrFE). The non-continuous morphology of P(VDF-TrFE) allows efficient charge extraction to the electrodes and avoids/reduces the piling up of photogenerated charges at the P(VDF-TrFE)/semiconductor interface. The switchable diode and photovoltaic enabled by the inserted ferroelectric dipoles may allow new applications of organic electronic devices.

Acknowledgements

The authors acknowledge the financial support by National Science Foundation under Award ECCS-1201384, the National Science Foundation MRSEC program (DMR 0820521), Nebraska EPSCoR Trans-disciplinary, Multi-Institutional Research Clusters Program, U.S. Department of Energy, Office of Basic Energy Sciences, Division of Materials Sciences and Engineering under Award DE-SC0004530.

References

1 L. Dou, J. You, J. Yang, C. C. Chen, Y. He, S. Murase, T. Moriarty, K. Emery, G. Li and Y. Yang, *Nat. Photonics*, 2012, **6**, 180.
2 G. Li, V. Shrotriya, J. S. Huang, Y. Yao, T. Moriarty, K. Emery and Y. Yang, *Nat. Mater.*, 2005, **4**, 864.
3 Z. He, C. Zhong, X. Huang, W.-Y. Wong, H. Wu, L. Chen, S. Su and Y. Cao, *Adv. Mater.*, 2011, **23**, 4636.

4 C. M. Amb, S. Chen, K. R. Graham, J. Subbiah, C. E. Small, F. So and J. R. Reynolds, *J. Am. Chem. Soc.*, 2011, **133**, 10062.
5 W. L. Ma, C. Y. Yang, X. Gong, K. Lee and A. J. Heeger, *Adv. Funct. Mater.*, 2005, **15**, 1617.
6 S. H. Park, A. Roy, S. Beaupre, S. Cho, N. Coates, J. S. Moon, D. Moses, M. Leclerc, K. Lee and A. J. Heeger, *Nat. Photonics*, 2009, **3**, 297.
7 B. Yang, J. Cox, Y. Yuan, F. Guo and J. Huang, *Appl. Phys. Lett.*, 2011, **99**, 133302.
8 T. Kirchartz, K. Taretto and U. Rau, *J. Phys. Chem. C*, 2009, **113**, 17958.
9 T. Kirchartz, B. E. Pieters, J. Kirkpatrick, U. Rau and J. Nelson, *Phys. Rev. B: Condens. Matter Mater. Phys.*, 2011, **83**, 115209.
10 H. Aarnio, P. Sehati, S. Braun, M. Nyman, M. P. de Jong, M. Fahlman and R. Osterbacka, *Adv. Energy. Mater.*, 2011, **1**, 792.
11 K. Vandewal, K. Tvingstedt, A. Gadisa, O. Inganäs and J. V. Manca, *Nat. Mater.*, 2009, **8**, 904.
12 Y. B. Yuan, T. J. Reece, P. Sharma, S. Poddar, S. Ducharme, A. Gruverman, Y. Yang and J. S. Huang, *Nat. Mater.*, 2011, **10**, 296.
13 B. Yang, Y. Yuan, S. Poddar, P. Sharma, R. Korlacki, S. Ducharme, A. Gruverman, R. Saraf and J. Huang, *Adv. Mater.*, 2012, **24**, 1455.
14 K. Asadi, P. de Bruyn, P. W. M. Blom and D. M. de Leeuw, *Appl. Phys. Lett.*, 2011, **98**, 183301.
15 Q. M. Zhang, H. Xu, F. Fang, Z.-Y. Cheng, F. Xia and H. You, *J. Appl. Phys.*, 2001, **89**, 2613.
16 J. Choi, C. N. Borca, P. A. Dowben, A. Bune, M. Poulsen, S. Pebley, S. Adenwalla, S. Ducharme, L. Robertson, V. M. Fridkin, S. P. Palto, N. N. Petukhova and S. G. Yudin, *Phys. Rev. B: Condens. Matter*, 2000, **61**, 5760.
17 M. Bai, M. Poulsen and S. Ducharme, *J. Phys.: Condens. Matter*, 2006, **18**, 7383.
18 M. Poulsen, A. V. Sorokin, S. Adenwalla, S. Ducharme and V. M. Fridkin, *J. Appl. Phys.*, 2008, **103**, 034116.
19 A. V. Bune, V. M. Fridkin, S. Ducharme, L. M. Blinov, S. P. Palto, A. V. Sorokin, S. G. Yudin and A. Zlatkin, *Nature*, 1998, **391**, 874.
20 M. Bai and S. Ducharme, *Appl. Phys. Lett.*, 2004, **85**, 3528.
21 T. Furukawa, T. Takahashi and T. Nakajima, *Curr. Appl. Phys.*, 2010, **10**, e62.
22 P. Sharma, T. J. Reece, S. Ducharme and A. Gruverman, *Nano Lett.*, 2011, **11**, 1970.
23 Z. Hu, M. Tian, B. Nysten and A. M. Jonas, *Nat. Mater.*, 2009, **8**, 62.
24 S. Y. Yang, J. Seidel, S. J. Byrnes, P. Shafer, C.-H. Yang, M. D. Rossell, P. Yu, Y.-H. Chu, J. F. Scott, I. J. W. Ager, L. W. Martin and R. Ramesh, *Nat. Nanotechnol.*, 2010, **5**, 143.
25 T. Choi, S. Lee, Y. J. Choi, V. Kiryukhin and S. W. Cheong, *Science*, 2009, **324**, 63.
26 P. Sharma, T. Reece, D. Wu, V. M. Fridkin, S. Ducharme and A. Gruverman, *J. Phys.: Condens. Matter*, 2009, **21**, 485902.
27 A. Hayakawa, O. Yoshikawa, T. Fujieda, K. Uehara and S. Yoshikawa, *Appl. Phys. Lett.*, 2007, **90**, 163517.
28 B. Zimmermann, U. Würfel and M. Niggemann, *Sol. Energy Mater. Sol. Cells*, 2009, **93**, 491.
29 M. O. Reese, A. J. Morfa, M. S. White, N. Kopidakis, S. E. Shaheen, G. Rumbles and D. S. Ginley, *Sol. Energy Mater. Sol. Cells*, 2008, **92**, 746.
30 C. Shuttle, R. Hamilton, B. O'Regan, J. Nelson and J. Durrant, *Proc. Natl. Acad. Sci. U. S. A.*, 2010, **107**, 16448.
31 C. M. Othon, F. B. Bateman and S. Ducharme, *J. Appl. Phys.*, 2005, **98**, 014106.